



CHORUS

This is the accepted manuscript made available via CHORUS. The article has been published as:

First-Principles Prediction of Metal-Free Magnetism and Intrinsic Half-Metallicity in Graphitic Carbon Nitride

Aijun Du, Stefano Sanvito, and Sean C. Smith

Phys. Rev. Lett. **108**, 197207 — Published 11 May 2012

DOI: [10.1103/PhysRevLett.108.197207](https://doi.org/10.1103/PhysRevLett.108.197207)

First Principles Prediction of Metal-free Magnetism and Intrinsic Half-Metallicity in Graphitic Carbon Nitride

*Aijun Du^{*1}, Stefano Sanvito² and Sean C. Smith³*

¹Centre for Computational Molecular Science, Australian Institute for Bioengineering and Nanotechnology, the University of Queensland, QLD 4072, Brisbane, Australia

²School of Physics and CRANN, Trinity College, Dublin 2, Ireland

³Centre for Nanophase Materials Sciences, Oak Ridge National Laboratory, Oak Ridge, Tennessee 37831, United States

ABSTRACT

Transition metal-free magnetism and half-metallicity has been recently the subject of an intense research activity due to its potential in spintronics application. Here we - for the first time - demonstrate via density functional theory that the most recently experimentally-realized graphitic carbon nitride (g-C₄N₃) displays a ferromagnetic ground state. Furthermore this novel material is predicted to possess an intrinsic half-metallicity ever reported to date. Our results highlight a new promising material toward realistic metal-free spintronics application.

PACS: 75.50.Dd, 75.20.Ck, 73.22.Pr, 71.20.Nr

* Corresponding authors: Aijun Du, Emails: a.du@uq.edu.au

Spintronics seeks at exploiting the electron spin in addition to the electrical charge for logic and memory devices and it is igniting a revolution in information processing [1]. A key challenge, stimulating innovation in this area, is the generation of 100 % spin-polarized currents at the Fermi level. A half metal, i.e., a material which filters the current into a single spin channel, fully meets this demand [2-3]. Up to now, half-metallicity has been shown in some materials such as manganese perovskites [4], Heusler compounds [5], metal-DNA complex [6], transition metal doped dilute magnetic semiconductor [7] and silicon nanowire/heterostructures [8-9]. In these materials, transition metals (TM) are believed to be responsible for the half metallicity. However, TM-contained systems may not be compatible with many current matured technologies, which mainly rely on main group semiconductor. Additionally, the large spin-coupling of TM atom will result in a very short spin relaxation time, greatly impacting on the performance of spintronics devices.

Recently, a single layer of graphite, i.e. 2D graphene has been attracted considerable research attentions due to its unique electronic properties [10-12]. When graphene is cut into 1D graphene nanoribbon, magnetism will be induced at the zigzag edge together with the finite size effect [13]. One of interesting application in relation to the magnetism of zigzag graphene nanoribbon is the novel half-metallicity in the presence of electric field as predicted by the Berkeley group [14]. This has opened an exciting pathway for the development of next-generation metal-free spintronics. However, the required in-plane electric field is too strong to be obtained in experiments [14-15]. Some new strategies have been proposed to realize such metal-free half-metallicity [16-29]. Kan et al. and Dutta et al. predicted half-metallicity in edge modified zigzag graphene nanoribbon by small organic molecule or B/N dopants, respectively [16-19]. Although these methods are successful in showing half-metallicity in the absence of electric field, it remains to be experimentally impractical because of the difficulties on the fine control positions of functional groups or B/N dopant. Hydrogenations of graphene or h-BN sheet have been also reported to be ferromagnetic and half-metallic [20-21], but the experimental realization

of hydrogenation is still a big challenge by the current technologies because they are often formed in a random way on a host structure. Most recently, ferroelectric poly(vinylidene fluoride) is found to be physisorbed onto graphene and the switching between half-metallic and insulating states can be achieved [22]. Hybrid *C/BN* nanotube [23] have been also predicted to be half-metallic due to an intrinsic chemical potential difference between the two boundaries [24]. Our group has also reported novel half-metallicity in finite-length nanotube nanodot [25] and vacancy contained *h-BN* monolayer [26]. Despite many interesting studies, metal-free half-metallicity has yet never experimentally reported in all the predicted systems [30]. The possible reasons would be that all the theoretically predicted half-metallicity in *C/BN based* compounds needs either the carefully selective doping [16-19] or strong external electric field [14-15, 25], which may make the experimental synthesis largely inaccessible.

Very recently, a novel method based on cross-linking nitrile-containing anions in ionic liquid was used by Dai's group to generate the functionalized carbon material [31]. The experimental synthesis involves the high temperature pyrolysis of ionic liquid and then the rearrangement of chemical bonds in the pyrolytic residue. The formed carbon networks possess high content of pyrindinic structural units, pointing out a new type of graphitic carbon nitride (*g-C₄N₃*) material (see Fig. 1a). Such a material is essentially C-doped graphitic *C₃N₄* [32]. The substitution of N atom with C atom in nonmagnetic *g-C₃N₄* will inject hole into the graphitic *C₃N₄* [32], which may significantly alter its electronic and magnetic properties. To explore this effect, standard density functional theory and state-of-the-art hybrid functional calculations have been carried out for the experimentally-synthesized *g-C₄N₃* materials. Remarkably, such a material displays a ferromagnetic ground state. Furthermore, its bandstructure is that of a half-metal, so that the material appears very promising for spintronics applications.

All the calculations on graphitic carbon nitride ($g\text{-C}_4\text{N}_3$) are performed by using the plane-wave basis Vienna Ab-initio Simulation Package (VASP) code [33] implementing the PBE exchange correlation functional [34]. An all-electron description, the projector augmented wave (PAW) method is used to describe the electron-ion interaction [35]. The cut-off energy for plane waves is chosen to be 500 eV and the vacuum space is at least 15 Å, which is large enough to avoid the interaction between periodical images. A $(7 \times 7 \times 1)$ Monkhorst–Pack grid is used for the sampling of Brillouin zone during geometry optimization and more than 50 K-points are used to obtain the accurate band-structure. All the atoms in the supercell were allowed to relax and the convergence of force was set to 0.002 eV/Å. Spin-polarization is included through all the calculations. Since standard density functional theory may fail to describe magnetism, state-of-the-art hybrid functional calculations based on HSE06 functional [36] have been also carried out to examine the magnetism and half-metallicity in a primitive $g\text{-C}_4\text{N}_3$ unit cell (computationally accessible).

The lattice constant of $g\text{-C}_4\text{N}_3$ is first calculated to be 4.84 Å. Then geometry optimization for a primitive (1×1) $g\text{-C}_4\text{N}_3$ is carried out by utilizing the conjugate gradient method. Figure 1a and 1b present a top and a side view of the fully relaxed (1×1) $g\text{-C}_4\text{N}_3$. The energy for spin-polarized solution (ferromagnetic state) is 0.1 eV lower than that in a non-spin-polarized calculation. The magnetic moment is found to be $1 \mu_B$ per formula unit and it is evenly distributed among three neighboring nitrogen atoms in a (1×1) $g\text{-C}_4\text{N}_3$ as will be shown in a magnetic charge density plot (Fig. 4c).

In order to explore the magnetic ground state of $g\text{-C}_4\text{N}_3$, an anti-ferromagnetic (AFM) configuration has been considered by using a (2×2) supercell. The geometry of such a supercell has been first optimized for a non-magnetic (NM), an anti-ferromagnetic (AFM) and a ferromagnetic configuration. Fig. 2 presents the equilibrium configurations, local magnetic arrangements and energetic for FM, AFM and NM states, respectively. Clearly, the ferromagnetic state (Fig. 2a) is found to be the most energetically stable, with energy 0.25 and 0.23 eV lower than that of the AFM and NM configurations,

respectively. The corresponding magnetic moment in a (2×2) supercell is calculated to be $4\mu_B$ for FM state. Such ferromagnetism may be understood by the fact that the pair of electrons (occupying a C-N bonding orbital) is broken up after injecting a hole in g-C₃N₄ around the substitutional N site. Interestingly, the (2×2) g-C₄N₃ structure is found to be reconstructed into a slightly distorted structure (see Fig. 1c and 1d) during the geometry optimization. The two N-atoms layers shift upward and downward with respect to the layer plane by around 0.30 Å (see Fig 1d), respectively. It is important to compare the relative stability between the (1×1) and (2×2) reconstructed structures. We found that the (2×2) reconstruction is energetically more stable by 0.042 eV per (1×1) unit cell, indicating that the magnetism is robust against geometry relaxation in the supercell.

Having studied the magnetic ground state of g-C₄N₃, it is important to calculate its detailed electronic structure. Fig. 3 presents the band-structure and spin-resolved total density of state (TDOS) for a (1×1) unreconstructed and a (2×2) reconstructed geometries (Fig. 1c and 1d), respectively. Remarkably, the spin-up channel (red) possesses a very large band gap (~ 2 eV), whereas the spin-down one (green) did not show a gap. Thus the charge transport is dominated by the spin-down electron and the current flow in such a system should be fully spin-polarized, i.e. half metallicity. Additionally, close examination of the top of valence band (see Fig3a and 3b) indicates that this receives contributions mainly from the planar p_y and p_x atomic orbitals.

Notably, such half metallicity is obtained without transition metals and without external stimuli, so that g-C₄N₃ appears as the first, experimentally synthesized, metal-free half-metal.

To further understand the physical origin of ferromagnetism and half-metallicity around the Fermi level in g-C₄N₃, a detailed analysis of orbital-resolved DOS has been carried out. Fig. 4a and 4b present the spin-resolved DOS projected on the p -orbitals of N and C for a (1×1) unreconstructed and a (2×2) reconstructed g-C₄N₃ materials, respectively. Clearly, the half-metallicity and magnetic moment are mainly attributed to the p -orbital of three N atoms. Fig. 4c and 4d plot top views of the 3D isosurface

for net magnetic charge density (electronic charge density difference between spin-up and spin-down channel, i.e. $\rho_{\uparrow} - \rho_{\downarrow}$) in a XOY plane. Similar to a (1×1) unreconstructed g-C₄N₃, the magnetic moments are also localized around N-atoms in a (2×2) reconstructed g-C₄N₃.

It is important to examine whether the experimentally fabricated g-C₄N₃ material is stable and whether the magnetic state survives at room temperature. In order to explore this aspect, a large (4×4) supercell containing 112 atoms is built and spin-polarized *ab initio* molecular dynamics simulations are performed with a Nose-Hoover thermostat either at 300K and 500K. Figure 6a and 6b show respectively the fluctuations in the temperature and the magnetic moment as a function of the simulation time at 300K. After 30ps we find no structure destruction of the g-C₄N₃ monolayer. This can be understood by the fact that the binding energies of the C-N and C-C bonds are much larger than the thermal energy corresponding to room temperature. Remarkably, the ground state remains magnetic with an average magnetic moment of around $13 \mu_B$ at 300K. Note however that such temperature does not correspond to a magnetic critical temperature as our molecular dynamics does not include spin-dynamics. As such our result simply establishes how robust is the magnetic moment against lattice deformation. Similar structural and magnetic stability is achieved in molecular dynamics simulations at 500K [show in Fig. 6c and 6d].

It is well known that general gradient approximation (PBE exchange correlation functional) will significantly underestimate the size of band gap. Hybrid functional such as HSE06 [36] is expected to perform very well in predicting the accurate gap and magnetic moment. Our previous work indicates band gap difference between DFT and hybrid functional methods can be as large as 1 eV in carbon based materials [37]. To explore this effect, state-of-the-art HSE06 functional calculations have been carried out for a (1×1) unreconstructed g-C₄N₃ system, which is largely computationally accessible. Fig. 5a and 5b present the calculated band structures and DOS, respectively. Clearly, both functional predicted similar dispersion curves for valence and conduction bands, respectively, but the position of

conduction bands is significantly up-shifted. Remarkably, we find that the ground state still remains ferromagnetic with the same magnetic moment ($1 \mu_B$) as that obtained by the PBE exchange correlation functional (see Fig 3). So the predicted intrinsic half-metallicity and ferromagnetism survive to the choice of functional.

In conclusion, based on first-principles simulations, we for the first time predicted that the most recently experimentally-realized g-C₄N₃ material [31] exhibits a ferromagnetic ground state and intrinsic half-metallicity. Here we should note that previously proposed strategies to realize metal-free half-metallicity may be hard to be experimentally controllable because strong external electric field or carefully selective doping is required. Our work thus reports on the first metal-free real half-metallic material, even though the experimental synthesis of pure g-C₄N₃ may still remain a challenge. As metal-free magnets potentially offers large spin relaxation times due to small spin-orbit coupling [38], our results highlight a new promising material for experimental validation studies toward the realistic metal-free spintronics application.

ACKNOWLEDGMENT

We acknowledge generous grants of high-performance computer time from the AIBN cluster computing facility at The University of Queensland and the Australian Research Council (LIEF grant LE0882357: A Computational Facility for Multiscale Modeling in Computational Bio and Nanotechnology), Queensland Cyber Infrastructure Foundation (QCIF) and the Australian Partnership for Advanced Computing National Facility. A.D. also greatly appreciate the QEII Fellowship and financial support of the Australian Research Council under Discovery Project (DP110101239). SS acknowledge Science Foundation of Ireland for financial support (07/IN.1/I945). SCS acknowledges support from the Center for Nanophase Materials Sciences, which is sponsored at the Oak Ridge National Laboratory by the Scientific User Facilities Division, US Department of Energy.

FIGURE CAPTIONS

Figure 1 (a) a top and side (b) view of the fully optimized (1 × 1) g-C₄N₃, (c) a top view and (d) a side view of a (2 × 2) reconstructed g-C₄N₃. Green and blue balls represent C and N atoms, respectively.

Figure 2 Magnetic moment and relative energies for (a) ferromagnetic (FM), (b) anti-ferromagnetic (AFM) and (c) non-magnetic (NM) states in a (2 × 2) reconstructed g-C₄N₃.

Figure 3 Band structure and spin-resolved total density of state for a (1×1) unreconstructed ((a) and (c)) and a (2×2) reconstructed ((b) and (d)) g-C₄N₃, respectively. The short dot line indicates the Fermi level.

Figure 4 Projected DOS on the p-orbital of N and C atoms [(a) and (b)] and 3D isosurface plots of magnetic charge density ($\rho_{\uparrow} - \rho_{\downarrow}$) for a (1 × 1) unreconstructed (a) and a (2×2) reconstructed g-C₄N₃ in the FM ground state. The short dot line indicates the Fermi level.

Figure 5 (a) Band structures and (b) DOS calculated by HSE06 functional for a (1 × 1) g-C₄N₃. The short dot line indicates the Fermi level.

Figure 6 The fluctuations of temperature (a) and ferromagnetic moment (b) as a function of molecular dynamic simulation step at 300K. (d) and (e) are similar to (a) and (b), respectively, but for another molecular dynamic run at 500K.

REFERENCES

- [1] S. A. Wolf et al., *Science* **294**, 1488 (2001).
- [2] D. D. Awschalom, and M. E. Flatt, *Nat. Phys.* **3**, 153 (2007).
- [3] C. Felser, G. H. Fecher, and B. Balke, *Angew. Chem. Int. Ed.* **46**, 668 (2007).
- [4] J.-H. Park et al., *Nature (London)* **392**, 794 (1998).
- [5] R. A. de Groot, F. M. Mueller, P.G. vanEngen, K.H.J. Buschow, *Phys. Rev. Lett.* **50**, 2024 (1983).
- [6] S. S. Mallajosyula and S. K. Pati, *J. Phys. Chem. B* **111**, 13 877 (2007)
- [7] J. E. Medvedeva, A. J. Freeman, X. Y. Cui, C. Stampfl, and N. Newman, *Phys. Rev. Lett.* **94**, 146602 (2005).
- [8] H.Wu, P. Kratzer, and M. Scheffler, *Phys. Rev. Lett.* **98**, 117202 (2007).
- [9] E. Durgun, D. Cakir, N. Akman, and S. Ciraci, *Phys. Rev. Lett.* **99**, 256806 (2007).
- [10] K. S. Novoselov et al., *Proc. Natl. Acad. Sci. U.S.A.* **102**, 10 451 (2005).
- [11] A. K. Geim and K. S. Novoselov, *Nature Mater.* **6**, 183 (2007).
- [12] K. S. Novoselov et al., *Nature (London)* **438**, 197 (2005).
- [13] Y. W. Son, M. L. Cohen, and S. G. Louie, *Phys. Rev. Lett.* **97**, 216803 (2006).

- [14] Y. W. Son, M. L. Cohen, and S. G. Louie, *Nature* **444**, 347 (2006).
- [15] E. J. Kan, Z. Y. Li, J. L. Yang, and J. G. Hou, *Appl. Phys. Letts.* **97**, 243116 (2007).
- [16] E. Kan et al., *J. Am. Chem. Soc.* **130**, 4224 (2008).
- [17] S. Dutta, A. K. Manna, and S. K. Pati, *Phys. Rev. Letts.* **102**, 096601 (2009).
- [18] S. Dutta, and S. K. Pati, *J. Phys. Chem. B* **112**, 1333 (2008).
- [19] Y. F. Li, Z. Zhou, P. W. Shen, and Z. F. Chen, *ACS Nano* **3**, 1952 (2009).
- [20] J. Zhou, Q. Wang, Q. Sun, X. S. Chen, Y. Kawazoe, and P. Jena, *Nano Letts.* **9**, 3867 (2009).
- [21] W. Chen et al., *J. Am. Chem. Soc.* **132**, 1699 (2010).
- [22] Y. L. Lee, S. Kim, C. Park, J. Ihm, and Y. W. Son, *ACS Nano* **4**, 1345 (2010).
- [23] A. J. Du, Y. Chen, Z. H. Zhu, G. Q. Lu, and S. C. Smith, *J. Am. Chem. Soc.* **131**, 1682 (2009).
- [24] B. Huang et al., *Appl. Phys. Letts.* **97**, 043115 (2010).
- [25] A. J. Du, Y. Chen, G. Q. Lu, and S. C. Smith, *Appl. Phys. Letts.* **93**, 073102 (2008).
- [26] A. J. Du, Y. Chen, Z. H. Zhu, R. Amal, G. Q. Lu, and S. C. Smith, *J. Am. Chem. Soc.* **131**, 17354 (2009).
- [27] E. J. Kan, X. J. Wu, Z. Y. Li, X. C. Zeng, J. L. Yang, and J. G. Hou, *J. Chem. Phys.* **129**, 084712 (2008).
- [28] F. W. Zheng et al., *Phys. Rev. B* **78**, 205415 (2008).
- [29] B. Huang et al., *Appl. Phys. Letts.* **97**, 043115 (2010).
- [30] A. J. Du, and S. C. Smith, *J. Phys. Chem. Letts.* **2**, 73, (2011).

- [31] J. S. Lee, X. Q. Wang, H. M. Luo, S. Dai, *Adv. Mater.* **22**, 1004 (2010).
- [32] E. Kroke, M. Schwarz, E. Horath-Bordon, P. Kroll, B. Noll, and A. D. Norman, *New J. Chem.* **26**, 508 (2002).
- [33] G. Kresse and J. Furthmuller, *Comput. Mater. Sci.* **6**, 15 (1996); *Phys. Rev. B* **54**, 11169 (1996).
- [34] J. P. Perdew, K. Burke, and M. Ernzerhof, *Phys. Rev. Letts.* **77**, 3865 (1996).
- [35] G. Kresse and D. Joubert, *Phys. Rev. B* **59**, 1758 (1999); P. E. Blochl, *Phys. Rev. B* **50**, 17953 (1994).
- [36] J. Heyd, G. E. Scuseria, M. Ernzerhof, *J. Chem. Phys.* **124**, 219906 (2006).
- [37] A. J. Du, Z. H. Zhu, and S. C. Smith, *J. Am. Chem. Soc.* **132**, 2876 (2010).
- [38] S. Sanvito, *Chem. Soc. Rev.* **40**, 336 (2011).

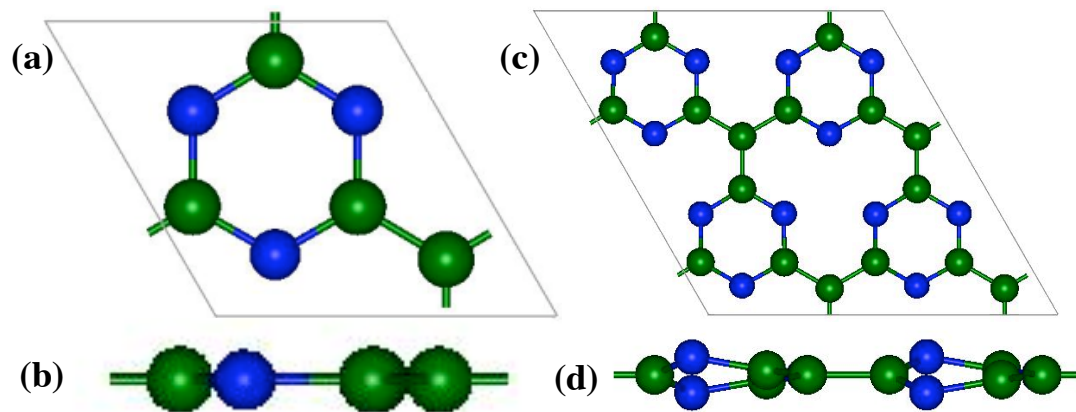


Figure 1 A. J. Du et al.

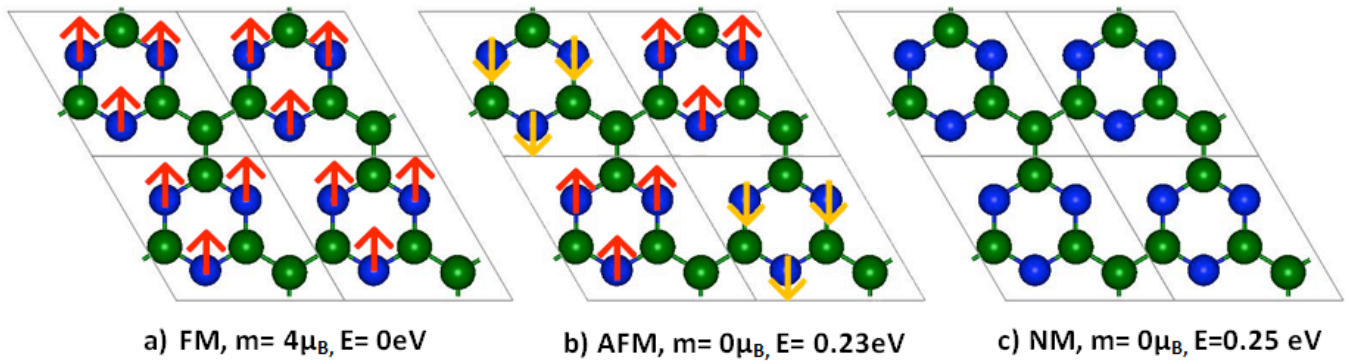


Figure 2 A. J. Du et al.

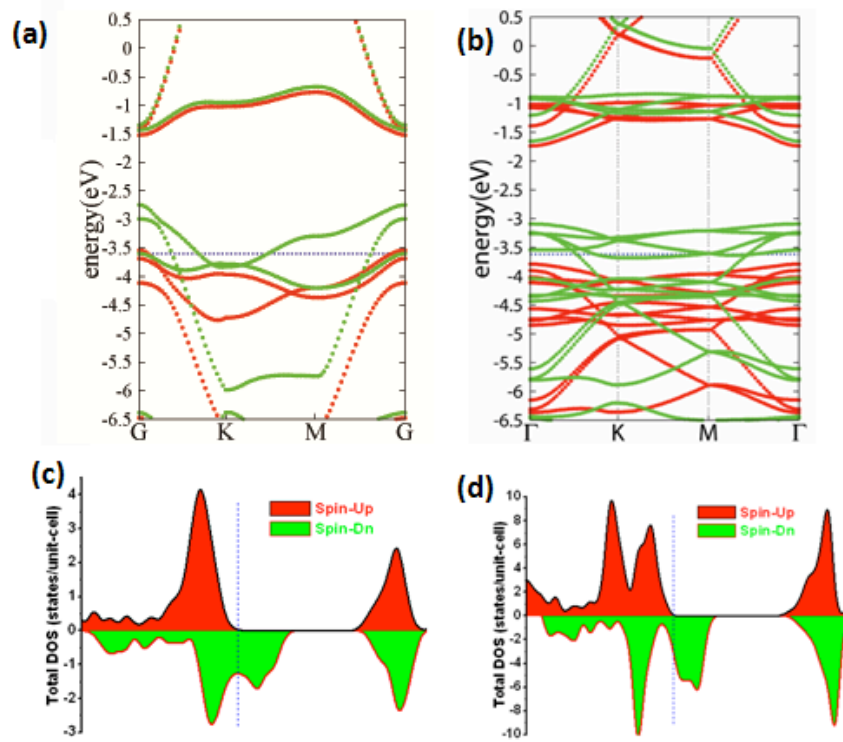


Figure 3 A. J. Du *et al.*

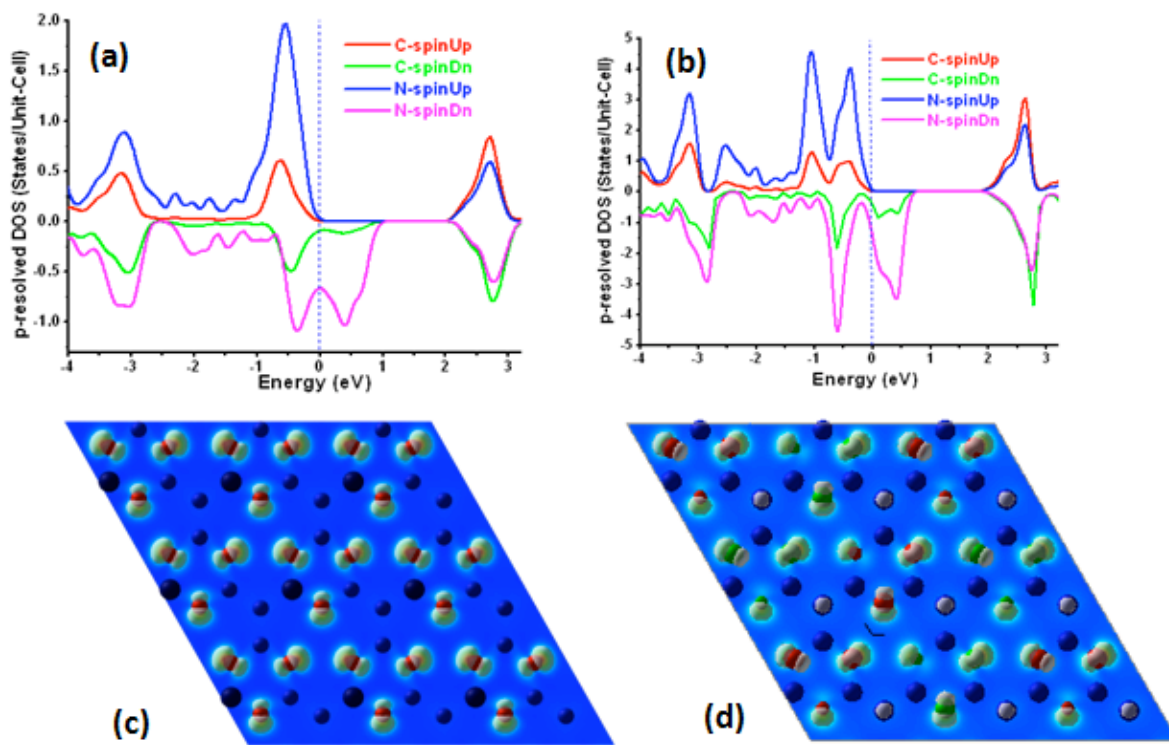


Figure 4 A. J. Du *et al.*

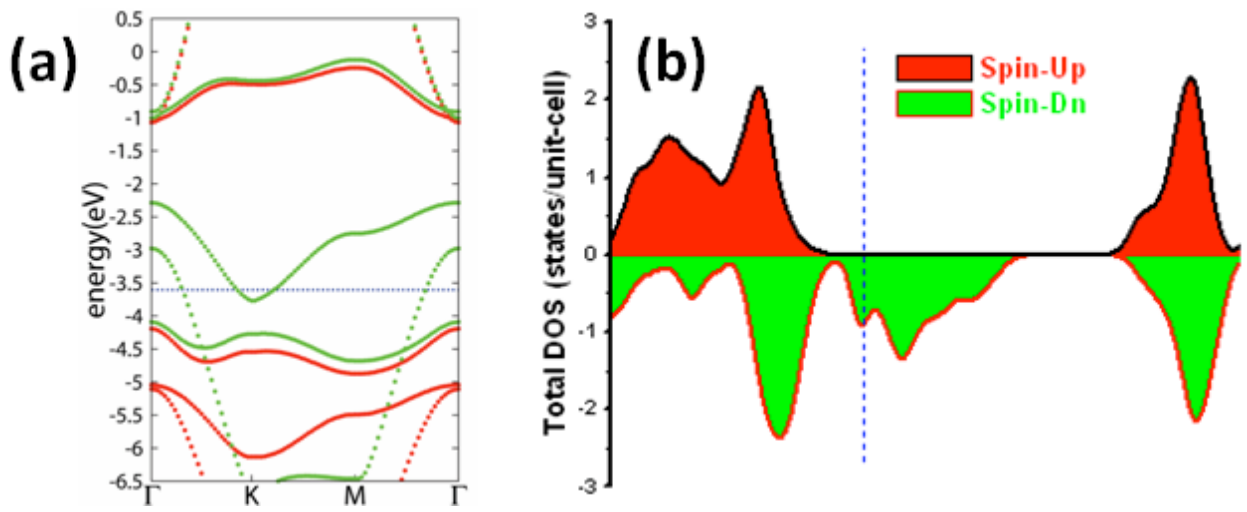


Figure 5 A. J. Du *et al.*

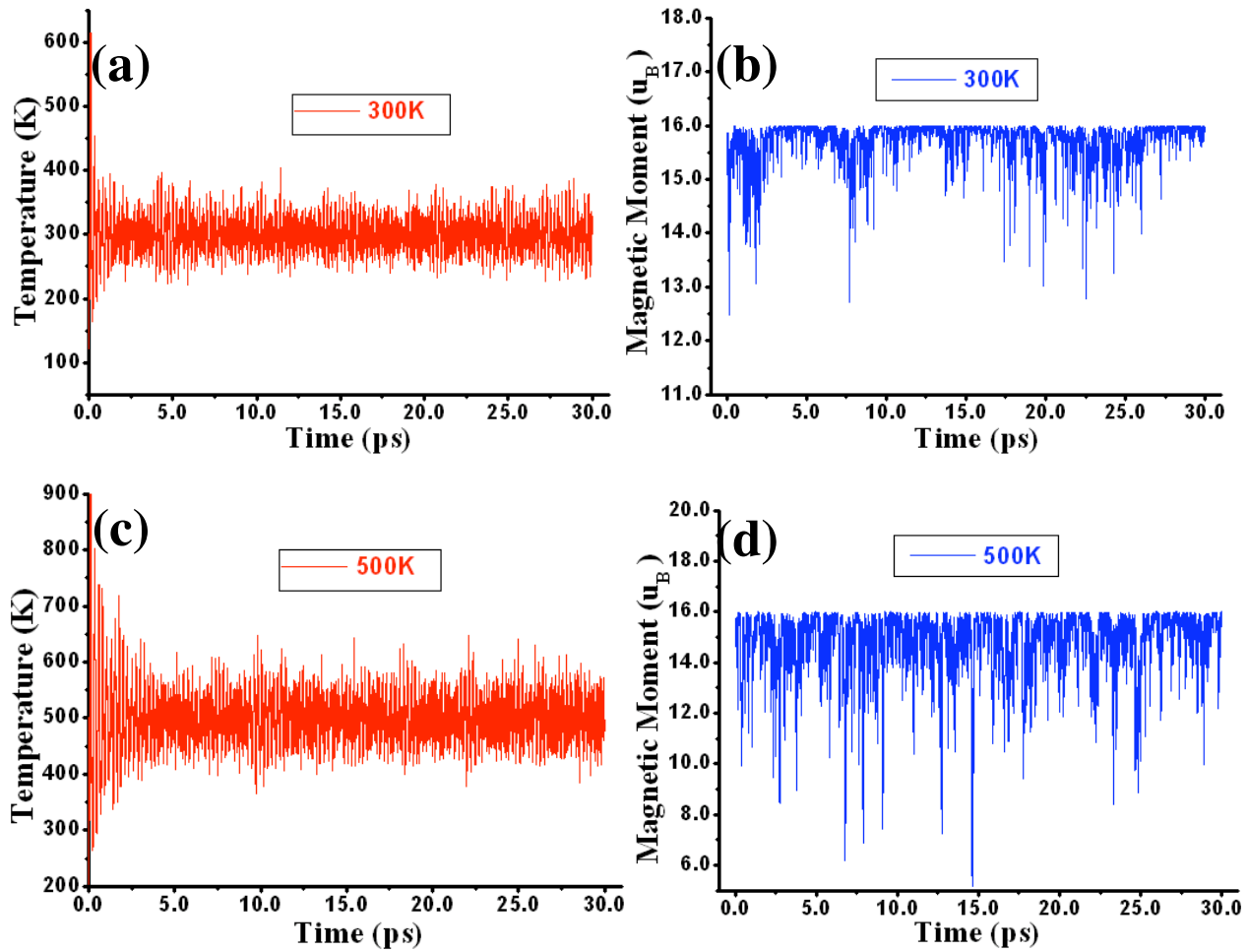


Figure 6 A. J. Du *et al.*